

# PCCP

Accepted Manuscript



This is an *Accepted Manuscript*, which has been through the Royal Society of Chemistry peer review process and has been accepted for publication.

*Accepted Manuscripts* are published online shortly after acceptance, before technical editing, formatting and proof reading. Using this free service, authors can make their results available to the community, in citable form, before we publish the edited article. We will replace this *Accepted Manuscript* with the edited and formatted *Advance Article* as soon as it is available.

You can find more information about *Accepted Manuscripts* in the [Information for Authors](#).

Please note that technical editing may introduce minor changes to the text and/or graphics, which may alter content. The journal's standard [Terms & Conditions](#) and the [Ethical guidelines](#) still apply. In no event shall the Royal Society of Chemistry be held responsible for any errors or omissions in this *Accepted Manuscript* or any consequences arising from the use of any information it contains.

## COMMUNICATION

# Direct Synthesis of Phosphorous and Nitrogen Co-Doped Monolayer Graphene with Air-Stable n-Type Characteristics†

Cite this: DOI: 10.1039/x0xx00000x

Yunzhou Xue,<sup>‡ab</sup> Bin Wu,<sup>‡a</sup> Hongtao Liu,<sup>a</sup> Jiahui Tan,<sup>a</sup> Wenping Hu<sup>a</sup> and Yunqi Liu<sup>\*a</sup>Received 00th January 2012,  
Accepted 00th January 2012

DOI: 10.1039/x0xx00000x

[www.rsc.org/](http://www.rsc.org/)

**Large-area substitutional phosphorous-nitrogen co-doped monolayer graphene is directly synthesized on Cu surface by chemical vapor deposition method using molecule of phosphonitrilic chloride trimer as the phosphorus and nitrogen sources. The doping levels of both phosphorus and nitrogen atoms show a decrease as a function of the growth temperature, in contrast, the doping effect is enhanced with temperature because of the formation of more stable bond configuration for dopants at higher temperature. Moreover, the doping amount of nitrogen atoms is always higher than that of phosphorus atoms at all used temperature. The phosphorus and nitrogen co-doped graphene exhibits the remarkable air-stable n-type characteristic. This work demonstrates the critical role of phosphorus atoms in achieving much enhanced capability of electron donation compared to nitrogen atom doping of graphene, and is important for various applications associated with the need of air stable n-type graphene materials.**

Materials engineering by structural and compositional modifications provides unlimited possibility to develop novel materials with desired properties. Graphene, a two-dimensional monolayer form of sp<sup>2</sup>-hybridized carbon densely packed into a honeycomb lattice structure,<sup>1</sup> has witnessed success in excellent physical properties<sup>2–8</sup> and outstanding stability at

ambient conditions.<sup>9</sup> The two-dimensional nature of graphene allows for the effective modifications of its chemical and physical properties by compositional and surface modifications without damaging its basal structural integration, significantly broadening the library of graphene-based materials and applications. For example, graphene under ambient condition usually exhibits p-type characteristic due to surface adsorption of water or oxygen molecules,<sup>10,11</sup> but its electrical properties of graphene can be changed from p-type to n-type by heteroatom substitution of carbon in graphene lattice<sup>12–19</sup> or surface adsorption of suitable donor molecules.<sup>20–22</sup> The n-type graphene itself is important for applications including lithium batteries,<sup>23–24</sup> electrochemical biosensing,<sup>25</sup> ultracapacitors,<sup>26–29</sup> and most importantly, the combination of p- and n-type graphene such as graphene p-n junctions could be used as a basic building block for graphene-based optoelectronic devices.<sup>30</sup> In this case, the extra electron and hole can be generated by a broadband light stimulation, and separated by built-in electric field for light harvesting applications. However, achieving air-stable n-type graphene has been proven to be challenging, as n-type behavior of most reported n-type graphene materials gradually disappear with extended exposure time due to the neutralization effect of surface adsorption of ambient molecules. This indicates that the majority electron density of produced n-type materials is too low to compensate the reverse p-doping effect from surface dopant doping.

Current methods for producing n-type graphene include surface adsorption of external donor molecules, graphene edge reaction with NH<sub>3</sub> at high temperature<sup>31</sup> and chemical vapor deposition (CVD) method using gas (NH<sub>3</sub>),<sup>12</sup> solid (melamine)<sup>15</sup> or liquid (pyridine)<sup>13,14,32</sup> as n-doping source. In general, surface doping approach (for example, triphenylphosphine,<sup>33</sup> triphenylamine,<sup>33</sup> p-toluenesulfonic acid<sup>21,22</sup> and so on were studied previously) is limited in small doping element concentration, leading to lightly doping, and

<sup>a</sup>Beijing National Laboratory for Molecular Sciences, Key Laboratory of Organic Solids, Institute of Chemistry, Chinese Academy of Sciences, Beijing 100190, P. R. China. E-mail: liuyq@iccas.ac.cn

<sup>b</sup>Institute of Functional Nano & Soft Materials (FUNSOM), Soochow University, Suzhou, Jiangsu 215123, P. R. China

<sup>‡</sup>These authors contributed equally to this work.

<sup>†</sup>Electronic supplementary information (ESI) available: SEM, optical microscopy, TEM, FET analyses of CVD obtained P, N-co-doped graphene. See DOI: 10.1039/x0xx00000x

subsequent encapsulation protection of graphene is also required to prevent the desorption or the change of surface donor spatial arrangement. Applying vacuum condition or thermal process could also damage graphene doping effect. Similar to conventional semiconductor industry, heteroatom substitution into graphene lattice is in principle a promising method to realize the stable doping effect with tunable doping density. Along this line, most studies have focused on introducing nitrogen atoms into graphene network by CVD method. Detailed study showed that nitrogen atom indeed replaced C atom in graphene lattice, and the electronic perturbation caused by a nitrogen dopant is localized near the dopant atom with 50–70% fraction of delocalized electrons.<sup>34</sup> However, the high nitrogen doping level is difficult to realize possibly due to high energy barrier by replacing C with N atoms, and the competition among spontaneous adsorbed donor doping, the low n-doping density and fraction of delocalized electrons results in a general problem that n-doping effect of graphene cannot be preserved at ambient condition.

Different from nitrogen atom, phosphorus atom has its valence electrons located in the third shell and has lower ionization energy compared with nitrogen atom, the features of which could enhance the doping capability by increasing the fraction of delocalized electrons per atom. It is also fundamentally interesting to know whether or not the disorder caused by incorporation of larger phosphorus atom into graphene lattice could destroy the graphene basal structure. Recently, post-synthesis doping phosphorus atom into pristine graphene has been investigated by rapid thermal annealing of phosphorus-contained compound sandwiched between two graphene layers, and it appeared that phosphorus doping allows for a strong n-doping effect compared to nitrogen doping.<sup>33</sup> However, this approach involves several processes to fabricate desired graphene doping structure, and the substitution doping mechanism is unclear. Moreover, rapid thermal annealing also seems to be difficult to scale up or modulate the dopant concentrations in a controlled manner. Direct synthesis of phosphorus doped graphene with air stable n-type characteristic by scaled-up CVD method is highly promising to overcome these difficulties, but has not been reported, and consequently various issues related to CVD process remained completely unknown.

Here we report for the first time the direct synthesis of large-area phosphorous-nitrogen co-doped monolayer graphene on Cu surface by CVD method with remarkable air-stable n-type characteristic. By using molecule of phosphonitrilic chloride trimer as the phosphorus and nitrogen sources, substitutional phosphorus and nitrogen doped monolayer graphene films were produced at various experimental conditions. It was found that, while the doping amount of both phosphorus and nitrogen atoms gradually decreased with the temperature, the whole doping effect enhanced with temperature due to more effective replacement of C with dopants at higher temperature. Moreover, we observed that the doping amount of nitrogen atoms were always higher than that of phosphorus atoms at all temperature used, reflecting their

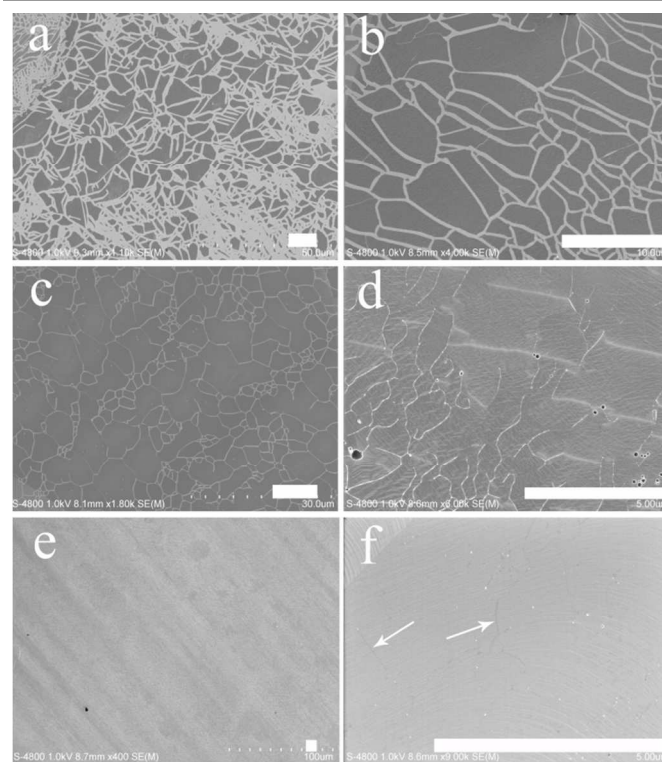


**Fig.1** SEM images of P, N-co-doped graphene grown on Cu surface for different growth time of 10 (a), 15 (b), 20 (c), 25 (d), 30 (e and f) min at 900 °C, respectively. The arrows in Figure 1f indicate the wrinkles of graphene on Cu surface. The scale bars are all 10 µm.

intrinsic relative ease to substitute C atoms in graphene lattice. The evaluation of electrical properties of our phosphorus and nitrogen co-doped graphene revealed the reliable n-type properties in air conditions, and the electron mobility reached 8–15 cm<sup>2</sup>/V·s, which is the average level of n-type graphene obtained by high temperature CVD method.

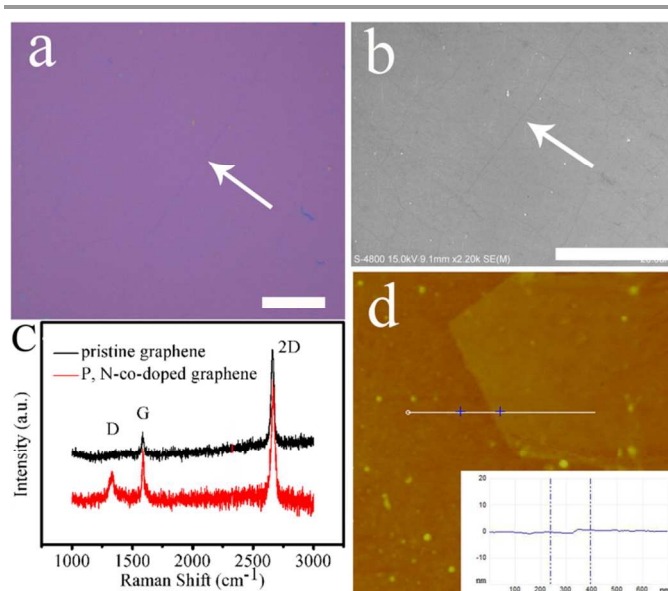
We chose a small molecule of phosphonitrilic chloride trimer containing both phosphorous and nitrogen elements to investigate the CVD growth process of doped graphene on Cu surface (Table S1). Exploring this system has advantages to clearly address the key questions such as whether phosphorous atoms can be incorporated into graphene lattice and the intrinsic density difference of two kinds of atoms existed in synthesized graphene. As schematically shown in Figure S1, the precursor molecule breaks down into single phosphorus and nitrogen atoms at high temperature, and then P, N and C atoms participates surface reaction to form monolayer P, N-co-doped graphene at high temperature at vacuum condition on Cu surface. In experiments, phosphonitrilic chloride trimer was dissolved in ethanol solution, and then was introduced into the reaction chamber by carrier gas.

Figure 1 shows the typical scanning electron microscopy (SEM) images of these products on Cu surface obtained at different growth stages. As the growth time increased from 10 min (Figure 1a), 15 min (Figure 1b), 20 min (Figure 1c), 25 min (Figure 1d) to 30 min (Figure 1e, f), the average size of individual doped graphene flakes separated by white Cu area

gradually increased and finally coalesced to form the seamless large-area film. This phenomenon is consistent with that happened in the growth of pristine graphene, indicating that the growth process of doped graphene also follows a surface nucleation and growth mode. Specifically, precursor molecules are first adsorbed on Cu surface, and then dissociated into the atomic form at the grown temperatures. These atoms combine with each other to form the cluster, i.e., nuclei that can be further grown into large flakes. Note that in contrast to well-defined shapes (hexagon or square) for graphene and nitrogen doped graphene observed in various cases, P, N-co-doped graphene flakes have no dominated geometric shape at explored experimental conditions, indicating that the disorder introduced by these doped atoms may alter the morphology of graphene flakes. After extended growth time (for example, 30 min shown in Figure 1e), the apertures among graphene flakes completely disappeared with uniform appearance. A closed-up SEM image of film in Figure 1f shows some black crooked lines marked by arrows, which can be attributed to the film wrinkles associated with the different thermal expansion coefficients between copper and film when the temperature decreased from 900 °C to room temperature. Interestingly, we noticed that the wrinkles of graphene on nickel and iron surface commonly appear white color in SEM images,<sup>11</sup> which is different from black-colored film wrinkles (See more examples in Figure S3) generally observed on Cu. This difference is general and may be due to the fact that graphene on nickel and iron surface are few-layer, and the heights of the wrinkles are higher than those of the monolayer graphene wrinkles on Cu surface. Further prolonging the growth time to 45 min, some black flakes appeared on film surface, which can be identified as the second layer graphene (Figure S4a). When the growth time reached 60 min, most of the Cu surface was covered by bilayer graphene (Figure S4b).

Figure 2a shows the optical image of the grown film transferred onto SiO<sub>2</sub>/Si substrate with 300 nm thick oxide layer, reflecting the grown large-area, continuous and uniform film. A place near the film edge was shown in Figure S5d for viewing, which distinguished the SiO<sub>2</sub>/Si substrate and the film. Figure 2b shows the SEM image of the same place with Figure 2a, and the same wrinkle can be clearly seen marked by the white arrow. More similar SEM images of monolayer graphene transferred onto SiO<sub>2</sub>/Si substrate were shown in Figure S5b and S5c. In addition, partially-covered graphene film with 25 min growth was also shown in Figure S5a, demonstrating that transferred film is preserved in its original structure in the presence of several white apertures.

Raman spectroscopy is an effective way to evaluate the layer number and the quality of graphene. We used the laser with 633 nm excitation wavelength to characterize the produced graphene film and the pristine graphene for comparison that was grown on Cu surface using methane CVD at 900 °C at low pressure condition. As shown in Figure 2c, the three most pronounced characteristic D, G and 2D bands for doped graphene appeared at locations of 1328, 1583 and 2664 cm<sup>-1</sup>, respectively. The D band is associated with defects in the



**Fig. 2** (a) Optical image of P, N-co-doped graphene transferred on 300 nm SiO<sub>2</sub>/Si substrate. The scale bar is 10 μm. (b) SEM image of graphene on SiO<sub>2</sub>/Si substrate which is the same place with Figure 2a. The white arrows mark the same wrinkle of graphene in Figures 2a and 2b, respectively. The scale bar is 20 μm. (c) Raman spectrum (633 nm laser wavelength) of pristine and P, N-co-doped graphene. (d) AFM image of P, N-co-doped graphene on SiO<sub>2</sub>/Si substrate. The image is 1.3 × 1.3 μm<sup>2</sup>. The bottom right inset shows the height profile along the white line, indicating the monolayer nature.

graphene or graphene edge, while the G band is the result of the first-order scattering of the E<sub>2g</sub> mode of sp<sup>2</sup> carbon domains.<sup>14</sup> The intensity ratio of D band and G band ( $I_D/I_G$ ) reflects the degree of defects in graphene or the edges. In our P, N-co-doped graphene, the  $I_D/I_G$  is about 0.57, higher than the pristine graphene (Figure 2c) and the average value of N-doped graphene, indicating the more topological defects introduced by the insertions of phosphorus atoms into sp<sup>2</sup> C lattice as compared with the case of nitrogen atoms. The 2D band, the second order zone boundary phonon mode for graphene and graphite, is the most important band to distinguish the layer number of graphene, and its shape and intensity are very sensitive to the layer numbers. In Figure 2c, the 2D band is a single and symmetric peak with a full width at half-maximum (FWHM) of 32 cm<sup>-1</sup>, which is the characteristic parameter for monolayer graphene. In addition, the intensity ratio of 2D band and G band ( $I_{2D}/I_G$ ) is about 2.6, further confirming the monolayer structure of our P, N-co-doped graphene. In addition, G and 2D peaks for pristine graphene are located at 1583 and 2660 cm<sup>-1</sup>, respectively, in which 2D peak is slightly downshifted compared to that of doped graphene, demonstrating the typical doping effect measured by Raman spectra.<sup>35,36</sup> Moreover,  $I_{2D}/I_G$  for doped graphene is smaller than that for pristine graphene, and corresponds to an estimation of electron doping level of  $>1 \times 10^{12}$  cm<sup>-2</sup>.<sup>35</sup> The atomic force microscopy (AFM) image (Figure 2d) collected at the edge of graphene film shows uniform appearance with a thickness about 0.804 nm, suggesting that the P, N-co-doped graphene is a monolayer film.

Figure 3 shows the X-ray photoelectron spectroscopy (XPS) results of the P, N-co-doped graphene on Cu surface under different growth temperatures. As shown in Figure 3a, the main C 1s peak is located at 284.8 eV, corresponding to the graphite-like  $sp^2$  C. Besides, a small peak located at 285.8 eV was clearly observed near the C 1s peak, corresponding to the C–N bonding structure with  $sp^2$  hybridized carbon, originating from the substitutional doping of N atoms. To further explore the relationship between P and N bonding type/content in the graphene and the growth temperature, four different temperatures 700, 800, 900 and 1000 °C were examined. As is known, the N atom bonding states can be distinguished as pyridine, pyrrole and graphitic nitrogen in graphene network, and the graphitic nitrogen is the most effective type to donate their additional electrons to the full graphene network. As shown in Figure 3b, with the temperature increasing, the existence type of N atoms in graphene changed evidently. Under 700 °C condition, the primary nitrogen type is pyridine nitrogen, pyrrole nitrogen followed and the least is the graphitic nitrogen. When the temperature increased to 800 °C, the nitrogen existed as pyrrole and graphitic nitrogen type and the content of them are almost the same. Further increasing the growth temperature to 900 °C, the main nitrogen type is the graphitic nitrogen and the pyridine nitrogen content is very little. The origin of the presence of this small peak at 900 °C is not clear at present, but may be related to the complex growth process that is not linearly dependent on the growth temperature. At last, when the temperature increased to 1000 °C, the nitrogen only existed as graphitic nitrogen, and the pyridine and pyrrole nitrogen completely disappeared.

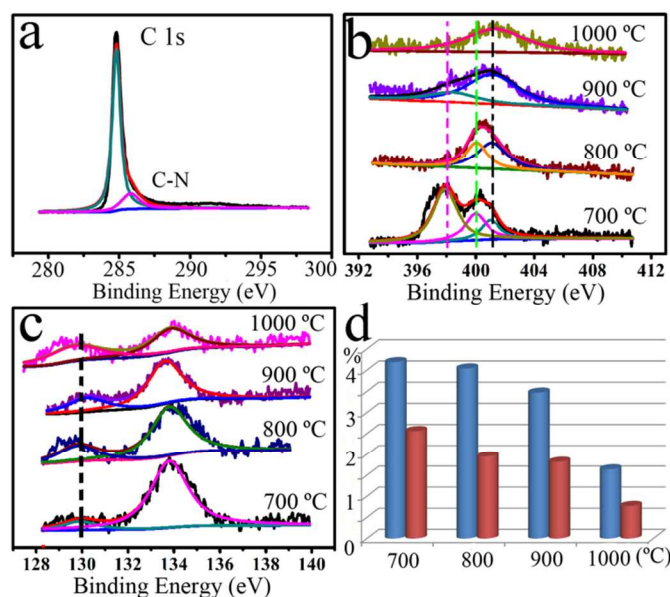


**Fig.3** (a–c) XPS spectra of P, N-co-doped graphene at different growth temperatures on Cu surfaces for C 1s, N 1s and P 1s peaks, respectively. (d) The histogram of N and P content at different growth temperature of 700, 800, 900 and 1000 °C. The blue and red cylinders represent N and P content, respectively.

For the phosphorus element, the main existence types are the P–C and P–O bonds which located at 130.0 eV and 133.8

eV, respectively. The presence of O elements was possibly due to physisorbed oxygen or decomposed ethanol. With the temperature increased from 700 to 1000 °C, the proportion of P–C bonds increased and the P–O bonds decreased, suggesting

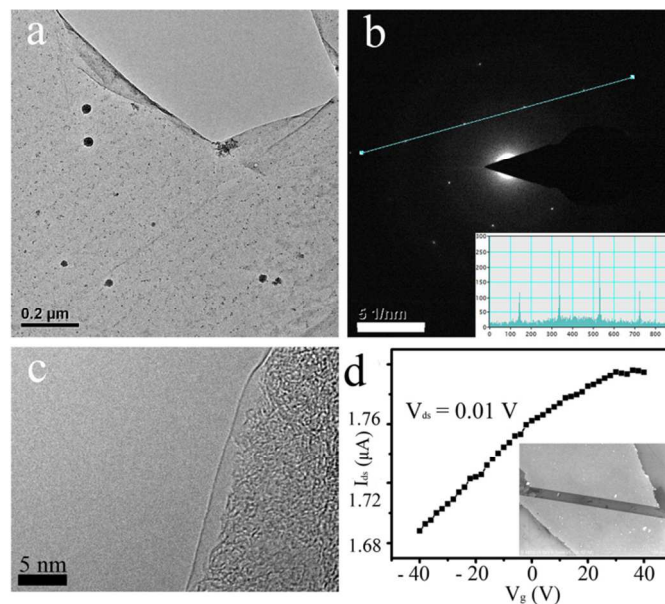


**Fig.4** (a) TEM image of P, N-co-doped graphene and the corresponding SAED pattern (b). The bottom right inset in Figure 2b shows the diffraction intensity taken along the 1-210 to -2110 axis of the pattern. (c) High resolution TEM image directly showing single layer edge. (d) Transfer characteristics of a typical P, N-co-doped graphene FET device measured in air. Note that Dirac point moves to a value less than -40 V that can not be observed. The inset shows a top view SEM image of a FET device.

that higher temperature benefits the effective doping for phosphorus atoms. In addition, XPS analysis (Figure 3d) provided strong evidence that the overall doping level for both phosphorous and nitrogen elements decreased with the temperature in the range of 700 to 1000 °C. This result is reasonable by considering the thermodynamical stability of C–C, C–N or C–P network formation, and is consistent with the observation for nitrogen doping by CVD method.<sup>17</sup> Note that the different stability would in principle result in a different probability of C–C, C–N and C–P formation, so the element ratio of the final doped product is not consistent with relative concentrations of each element existed in the reaction system. Moreover, a rapid drop of doping level for both P and N elements with the temperature increased from 900 to 1000 °C was observed, and this indicates that doping level is non-linearly dependent on growth temperature, which can be understood in the Boltzmann statistical principle. To ensure the quality and the P/N content in graphene network, the samples grown at 900 °C were chosen for further characterizations in this work.

The obtained P, N-co-doped graphene samples were also directly transferred onto Cu grids for further transmission electron microscopy (TEM) characterization. As shown in the low magnification TEM image (Figure 4a), the broken edge of P, N-co-doped graphene membrane tends to scroll. To

determine sample's crystallinity, the selected area electron diffraction (SAED) patterns were taken on different locations of the film as shown in Figure 4b, which displays the typical hexagonal crystalline structure of graphene. The SAED pattern confirmed that the doped graphene film still remained well ordered crystalline structures although large-sized P atoms could introduce additional disorder in the graphene network. Besides, the SAED images further confirmed that the P, N-co-doped graphene is monolayer as the {1100} six spots appear to be intense relative to the {2110} spots. The diffracted intensity taken along the 1-210 to -2110 axis for the pattern was shown in the right bottom inset in Figure 4b, giving the intense ratio  $I_{\{1100\}}/I_{\{2110\}} = 2.5$  that is characteristic of the monolayer graphene. Figure 4c shows the higher resolution TEM image of the folded edge as shown in Figure 4a, accurately confirming the monolayer nature of doped graphene film. For graphene samples with longer growth time, bilayer graphene was identified by both high resolution TEM image of edge (Figure S6d) and the value (about 1, Figure S6c) of intense ratio  $I_{\{1100\}}/I_{\{2110\}}$ .<sup>37–39</sup>

To investigate the electrical property of the obtained P, N-co-doped graphene, back-gate field-effect transistors (FETs) were fabricated on 300 nm SiO<sub>2</sub>/Si substrates with Au as the source/drain electrodes and doped silicon as the back gate. The device fabrication and process is described in experiment section, and a SEM image for a typical device was shown in the right bottom inset in Figure 4d. Figure 4d and Figure S7 show typical n-type transfer and output curves of the P, N-co-doped graphene device measured in air at room temperature. Note that the samples usually were exposed to air for several days during the processes involving doped graphene transfer, device fabrications and measurements, and the results for the same device remained essentially the same by repeated measurements. As is seen in Figure 4d, the Dirac point of doped graphene moved to a negative bias less than -40 V beyond the applied gate voltage range. This negative value of Dirac point is much smaller than -26 V for high nitrogen doping (~16.7%) graphene using the same device fabrication and measurement method in air,<sup>14</sup> and is in sharp contrast to most of nitrogen-doped graphene as they cannot exhibit n-type behavior in air. Note that the estimated values of the overall nitrogen doping and phosphorus doping from XPS data are about 4.5% and 2.5%, respectively, which are much lower than nitrogen-doped graphene grown by pyridine molecules.<sup>14</sup> The fact that this low phosphorus doping level produces air-stable n-type behavior is remarkable, demonstrating a key role of doped P atoms in significantly enhancing doping efficiency compared to nitrogen doping and also pointing out a much efficient doping approach for various specific applications. In addition, the measured electron mobility of our devices were found to be in the range of 8–15 cm<sup>2</sup>V<sup>-1</sup>s<sup>-1</sup>, which were in accordance with the nitrogen-doped graphene synthesized by CVD method at high temperature reported before.<sup>12–14,17</sup>

In summary, we have developed for the first time a facial CVD route to directly synthesize P, N-co-doped monolayer graphene using a molecule of phosphonitrilic chloride trimer as

phosphorus and nitrogen sources on Cu surface. The P, N-co-doped graphene exhibits a remarkably stable n-type behavior at ambient condition and a reasonable charge carrier mobility. This work demonstrates the role of P atoms in achieving much enhanced capability of electron donation compared to nitrogen atom doping of graphene, and is important for various applications associated with the need of air stable n-type graphene materials.

## EXPERIMENTAL SECTION

The P, N-co-doped graphene were produced on Cu surface using phosphonitrilic chloride trimer (P<sub>3</sub>N<sub>3</sub>Cl<sub>6</sub>, Sigma-Aldrich, CAS: 940-71-6) as the P and N sources, and the ethanol as the C source at various conditions. The phosphonitrilic chloride trimer was first dissolved in ethanol to reach saturated solution. The solution was then dropped into a plastic centrifugal tube with a small hole on the side wall. After that, the centrifugal tube was placed in the upstream of the quartz tube without the heating area. Before heating, 500 sccm high pure Ar was introduced into the system for 30 min to remove the air. Then 300 sccm Ar and 100 sccm H<sub>2</sub> were introduced into the furnace and the furnace was heated to aimed temperature. During the growth stage, the Ar gas is turned off and the H<sub>2</sub> gas is switched to 15–20 sccm while turning on the mechanical pump to keep the pressure of the quartz tube to 200–300 Pa for specified time. Finally, the furnace and pump are turned off and the system is introduced with the Ar gas until the pressure reaches the ambient condition.

Graphene FET device fabrication is as follows: individual organic ribbon was picked up by a mechanical probe and placed over the graphene as an “organic ribbon mask”. After that, Au source and drain electrodes (20–30 nm) were deposited on the P, N-co-doped graphene by thermal deposition. Finally, the “organic ribbon mask” was peeled off using a mechanical probe. In this way, P, N-co-doped graphene contacted with source and drain electrodes could be found and tested with Keithley 4200 at room temperature in air condition. The mobility of graphene charge carriers is extracted from the equation

$$\mu_{dev} = \frac{L}{V_D C_{ox} W} \cdot \frac{dI_D}{dV_G}$$

where L and W are the device channel length and width, V<sub>D</sub> is the voltage between source and drain electrodes, and C<sub>ox</sub> (C<sub>ox</sub> = 11 nF) is the gate capacitance per unit area.

## Characterizations

The samples were characterized by scanning electron microscopy (SEM, Hitachi S-4800, 1 KV and 15 KV), Raman spectroscopy (Renishaw inVia plus, with laser excitation of 633 nm), atomic force microscopy (AFM, Veeco Nanoman VS in the tapping mode), Transmission electron microscopy (TEM), X-ray photoelectron spectroscopy (XPS) and optical microscopy.

## ACKNOWLEDGEMENTS

This work was supported by the National Basic Research Program of China (2013CB933500, 2011CB932700 and 2011CB932303), by the National Natural Science Foundation of China (61171054, 21273243, 60911130231, 51233006 and 61390502), and Chinese Academy of Sciences.

## Notes and references

- K. S. Novoselov, A. K. Geim, S. V. Morozov, D. Jiang, Y. Zhang, S. V. Dubonos, I. V. Grigorieva and A. A. Firsov, *Science*, 2004, **306**, 666.
- K. S. Kim, et al. *Nature*, 2009, **457**, 706.
- K. S. Novoselov, E. McCann, S. V. Morozov, V. I. Falko, M. I. Katsnelson, U. Zeitler, D. Jiang, F. Schedin and A. K. Geim, *Nat. Phys.*, 2006, **2**, 177.
- N. Tombros, C. Jozsa, M. Popinciuc, H. T. Jonkman and B. J. Wees, *Nature*, 2007, **448**, 571.
- K. I. Bolotin, K. J. Sikes, Z. Jiang, M. Klima, G. Fudenberg, J. Hone, P. Kim and H. L. Stormer, *Solid State Commun.*, 2008, **146**, 351.
- K. S. Novoselov, A. K. Geim, S. V. Morozov, D. Jiang, M. I. Katsnelson, I. V. Grigorieva, S. V. Dubonos and A. A. Firsov, *Nature*, 2005, **438**, 197.
- Y. B. Zhang, Y. W. Tan, H. L. Stormer and P. Kim, *Nature*, 2005, **438**, 201.
- X. Du, I. Skachko, A. Barker and E. Y. Andrei, *Nat. Nanotechnol.*, 2008, **3**, 491.
- A. K. Geim and I. V. Grigorieva, *Nature*, 2013, **499**, 419.
- F. Schenin, A. K. Geim, S. V. Morozov, E. W. Hill, P. Blake, M. I. Katsnelson and K. S. Novoselov, *Nat. Mater.*, 2007, **6**, 652.
- Y. Z. Xue, B. Wu, Y. L. Guo, L. P. Huang, L. Jiang, J. Y. Chen, D. C. Geng, Y. Q. Liu, W. P. Hu and G. Yu, *Nano Res.*, 2011, **4**, 1208.
- D. C. Wei, Y. Q. Liu, Y. Wang, H. L. Zhang, L. P. Huang and G. Yu, *Nano Lett.*, 2009, **9**, 1752.
- Z. Jin, J. Yao, C. Kittrell and J. M. Tour, *ACS Nano*, 2011, **5**, 4112.
- Y. Xue, B. Wu, L. Jiang, Y. Guo, L. Huang, J. Chen, J. Tan, D. Geng, B. Luo, W. Hu, G. Yu and Y. Liu, *J. Am. Chem. Soc.*, 2012, **134**, 11060.
- Z. Sun, Z. Yan, J. Yao, E. Beitler, Y. Zhu and J. M. Tour, *Nature*, 2010, **468**, 549.
- Y. F. Lu, S. T. Lo, J. C. Lin, W. Zhang, J. Y. Lu, F. H. Liu, C. M. Tseng, Y. H. Lee, C. T. Liang and L. J. Li, *ACS Nano*, 2013, **7**, 6522.
- C. Zhang, L. Fu, N. Liu, M. Liu, Y. Wang and Z. Liu, *Adv. Mater.*, 2011, **23**, 1020.
- X. Li, H. Wang, J. T. Robinson, H. Sanchez, G. Diankov and H. Dai, *J. Am. Chem. Soc.*, 2009, **131**, 15939.
- D. W. Chang, E. K. Lee, E. Y. Park, H. Yu, H. J. Choi, I. Y. Jeon, G. J. Sohn, D. Shin, N. Park, J. H. Oh, L. Dai and J. B. Baek, *J. Am. Chem. Soc.*, 2013, **135**, 8981.
- X. Dong, D. Fu, W. Fang, Y. Shi, P. Chen and L. J. Li, *Small*, 2009, **5**, 12, 1422.
- A. K. Singh, M. Ahmad, V. K. Singh, K. Shin, Y. Seo and J. Eom, *ACS Appl. Mater. Interfaces*, 2013, **5**, 5276.
- A. K. Singh, M. W. Iqbal, V. K. Singh, M. Z. Iqbal, J. H. Lee, S. H. Chun, K. Shin and J. Eom, *J. Mater. Chem.*, 2012, **22**, 15168.
- A. L. M. Reddy, A. Srivastava, S. R. Gowda, H. Gullapalli, M. Dubey and P. M. Ajayan, *ACS Nano*, 2010, **4**, 6337.
- C. Zhang, N. Mahmood, H. Yin, F. Liu and Y. Hou, *Adv. Mater.*, 2013, **25**, 4932.
- Y. Wang, Y. Shao, D. W. Matson, J. Li and Y. Lin, *ACS Nano*, 2010, **4**, 1790.
- H. M. Jeong, J. W. Lee, W. H. Shin, Y. J. Choi, H. J. Shin, J. K. Kang and J. W. Choi, *Nano Lett.*, 2011, **11**, 2472.
- Z. Wen, X. Wang, S. Mao, Z. Bo, H. Kim, S. Cui, G. Lu, X. Feng, and J. Chen, *Adv. Mater.*, 2012, **24**, 5610.
- L. L. Zhang, X. Zhao, H. Ji, M. D. Stoller, L. Lai, S. Murali, S. McDonnell, B. Cleveger, R. M. Wallace and R. S. Ruoff, *Energy Environ. Sci.*, 2012, **5**, 9618.
- L. Zhao, L. Z. Fan, M. Q. Zhou, H. Guan, S. Qiao, M. Antonietti and M. M. Titirici, *Adv. Mater.*, 2010, **22**, 5202.
- K. Yan, D. Wu, H. Peng, L. Jin, Q. Fu, X. Bao and Z. Liu, *Nat. Commun.*, 2012, **3**, 1280.
- X. Wang, X. Li, L. Zhang, Y. Yoon, P. K. Weber, H. Wang, J. Guo and H. Dai, *Science*, 2009, **324**, 768.
- G. Imamura and K. Saiki, *J. Phys. Chem. C*, 2011, **115**, 10000.
- S. Some, J. Kim, K. Lee, A. Kulkarni, Y. Yoon, S. Lee, T. Kim and H. Lee, *Adv. Mater.*, 2012, **24**, 5481.
- L. Y. Zhao, R. He, K. T. Rim, T. Schiros, K. S. Kim, H. Zhou, C. Gutierrez, S. P. Chockalingam, C. J. Arguello, L. Palova, D. Nordlund, M. S. Hybertsen, D. R. Reichman, T. F. Heinz, P. Kim, A. Pinczuk, G. W. Flynn and A. N. Pasupathy, *Science*, 2011, **333**, 999.
- A. Das, S. Pisana, B. Chakraborty, S. Piscanec, S. K. Saha, U. V. Waghmare, K. S. Novoselov, H. R. Krishnamurthy, A. K. Geim, A. C. Ferrari and A. K. Sood, *Nat. Nanotechnol.*, 2008, **3**, 210.
- L. Wang, B. Wu, J. Chen, H. Liu, P. Hu and Y. Q. Liu, *Adv. Mater.*, 2014, **26**, 1559.
- S. Stankovich, D. A. Dikin, G. H. B. Dommett, K. M. Kohlhaas, E. J. Zimney, E. A. Stach, R. D. Piner, S. T. Nguyen and R. S. Ruoff, *Nature*, 2006, **442**, 282.
- Y. Hernandez, V. Nicolosi, M. Lotya, M. Blighe, Z. F. Sun, S. De, I. T. McGovern, B. Holland, M. Byrne, Y. K. Gun, Ko, J. J. Boland, P. Niraj, G. Duesberg, S. Krishnamurthy, R. Goodhue, J. Hutchison, V. Scardaci, A. C. Ferrari and J. N. Coleman, *Nat. Nanotechnol.*, 2008, **3**, 563.
- J. C. Meyer, A. K. Geim, M. I. Katsnelson, K. S. Novoselov, T. J. Booth and S. Roth, *Nature*, 2007, **446**, 60.